# Multi-method geophysical assessment of a shallow complex landslide

*Mohammadyar* Rahimi[1], *Clinton* Wood[2*], and *Salman* Rahimi[3]

[1]*Graduate Research Assistant, University of Arkansas, Fayetteville, AR, USA*
[2]*Associate Professor, University of Arkansas, Fayetteville, AR, USA*
[3]*Consulting Engineer, Arup, Oakland, CA, USA*
[*]*Corresponding author: cmwood@uark.edu*

## ABSTRACT

This study demonstrates the value of combining multiple non-invasive geophysical methods through a case study at a landslide along Highway 7 near Jasper, Arkansas, USA. Geophysical testing was conducted using Multichannel Analysis of Surface Waves (MASW), Horizontal to Vertical Spectral Ratio (HVSR), and Electrical Resistivity Tomography (ERT) along with select borings. Geophysical testing was aimed to provide a high-resolution and almost continuous image of subsurface conditions (including bedrock depth) for the slide area and to locate the groundwater table/highly saturated zones within the slide area which contribute to the slope movement. MASW revealed a highly variable depth to the weathered bedrock along the observed zone of displacement becoming shallower downslope. ERT detected saturated zones associated with observed seeps and springs in the area which were feeding water into the unstable zone. A low resistivity zone on the north side correlated to wet spots, while south of the highway saturation occurred near the deeper bedrock interface. Additionally, using a grid pattern HVSR approach, a high-resolution image of the shallow and complex bedrock topography was generated across the slide area providing valuable information for the repair design. Overall, the results of the combined geophysical approach provide a high-resolution image of landslide subsurface conditions which is critical for stability analyses and slope repair design. This integrated geophysical approach offers a more sustainable, rapid, and cost-effective solution for comprehensive landslide characterization and slope stability assessment when combined with conventional methods.

**Keywords:** Landslide; geophysics; subsurface imaging.

## 1. Introduction

Landslides represent major geologic hazards that incur substantial serviceability issues and economic losses annually across transportation networks, infrastructure, and buildings worldwide (Petley 2012). Characterizing landslide geometry, hydrogeological regime, movement kinematics, and failure mechanisms constitutes a critical step for hazard analysis, monitoring, remediation, and mitigation measures (Jongmans and Garambois 2007). However, conventional site investigation techniques like costly boreholes provide only discrete subsurface data at isolated locations that fail to capture the innate 3D complexities of many landslides tied to slope morphology, geology, hydrology, and seismology, which can be better characterized with 2D or 3D geophysical methods at a lower cost. Furthermore, even in some situations the conventional investigation is not feasible due to steep slopes or safety issues due to an active landslide. Following the geophysical measurements, an optimized drilling campaign can be conducted through geophysical surveys by guiding targeted borehole placement and depths to achieve subsurface validation using minimal sampling.

Recent advances in non-invasive geophysical methods furnished rapid wide area scanning tools to image landslide structure at higher resolutions critical for predictive modelling. Seismic methods like Multichannel Analysis of Surface Wave (MASW) have been employed to determine the subsurface layering and soil/rock interface, elastic dynamic properties, and stiffness variations indicative of slip surface geometry (Harba 2019, Hussain et al. 2020, Rahimi et al. 2021). Electrical Resistivity Tomography (ERT) can map stratigraphic information, soil type, internal seepage pathways and variable saturation zones leading to separation between moving soil material and below more stable hard rock (Samodra 2020, Imani et al. 2021). Ambient vibration techniques such as Horizontal to Vertical Spectral Ratio (HVSR) can estimate soil thickness overlaying bedrock as complementary information governing failure plane development particularly for landslides with shallow bedrock (Alonso-Pandavenes 2023, Ávila-Barrientos 2023). However, further research is still needed on actual case studies across various landslide situations to standardize overall procedures and reveal advantages and possible limitations of geophysical methods.

Integrating different geophysical datasets provides improved subsurface constraint to overcome individual limitations and ambiguities (Bichler et al. 2004). Joint structural models better inform slope stability analyses by reducing reliance on sparse direct sampling. Here the value of a combined MASW, ERT, and HVSR geophysical approach verified with limited borehole investigation is demonstrated for comprehensive

landslide characterization through a case study along Highway 7 near Jasper, Arkansas. Testing aimed to provide a high-resolution image of bedrock morphology, hydrogeology, and saturated zones contributing to the slope failure. Results highlighted the potential of integrated geophysics for more reliable and efficient landslide investigation essential for hazard mitigation planning.

## 2. Site location and geology

The slope area tested in this study is located along Arkansas Highway 7 near Jasper, Newton County, Arkansas. The city of Jasper, Arkansas is situated within the Salem Plateau region of the Ozark Highlands physiographic province (Adamski et al. 1995). The Ozark province encompasses much of southern Missouri and northern Arkansas and formed through uplift of a broad asymmetrical dome during the Ouachita orogeny in the early to middle Paleozoic Era. Lithology of the plateau consists predominantly of nearly horizontal sedimentary bedrock layers of limestone, dolomite, sandstone, and shales that gently dip away from the St. Francois Mountains toward the Arkansas River Valley (Braden 2015). These cherty carbonate units have been differentially weathered into a mature topography characterized by open ridges divided by steep V-shaped valleys (Adamski et al. 1995). Soils are generally thin, stony residuum weathered from the local bedrock. Additionally, minor faults and localized karst terrain associated with groundwater and bedrock fracturing contribute to surface and subsurface heterogeneity across the plateau landscape.

Observing a distress crack on the pavement approximately along the highway axis prompted geotechnical investigation regarding stability of the adjacent slope. The area exhibits variable slope; however, the primary slope orientation runs approximately north-to-south, almost perpendicular to the observed pavement fracture orientation.

## 3. Geophysical investigations

To characterize subsurface factors potentially contributing to the pavement distress and slope instability, a geophysical investigation program including MASW, HVSR, and ERT were performed along different lines perpendicular and parallel to the slope. Tests were performed in four days, Feb 1 and 5, 2021 and Mar 8 and 10, 2021. The ground conditions were moist although there was no rain prior to the testing. Three MASW survey lines, Five ERT survey lines, and approximately 100 HVSR measurements acquired along the MASW and ERT lines in a grid pattern within the slide. The exact locations of the geophysical field measurements along with the four boring locations B1-B4 are shown in Figure 1. However, as the boreholes B1 and B3 are far from the MASW lines they are not included in the 2D cross sections. The location of the surface crack on the pavement and direction of landslide movement is shown in Figure 2. The testing parameters and data processing workflow are presented in detail for each method below.

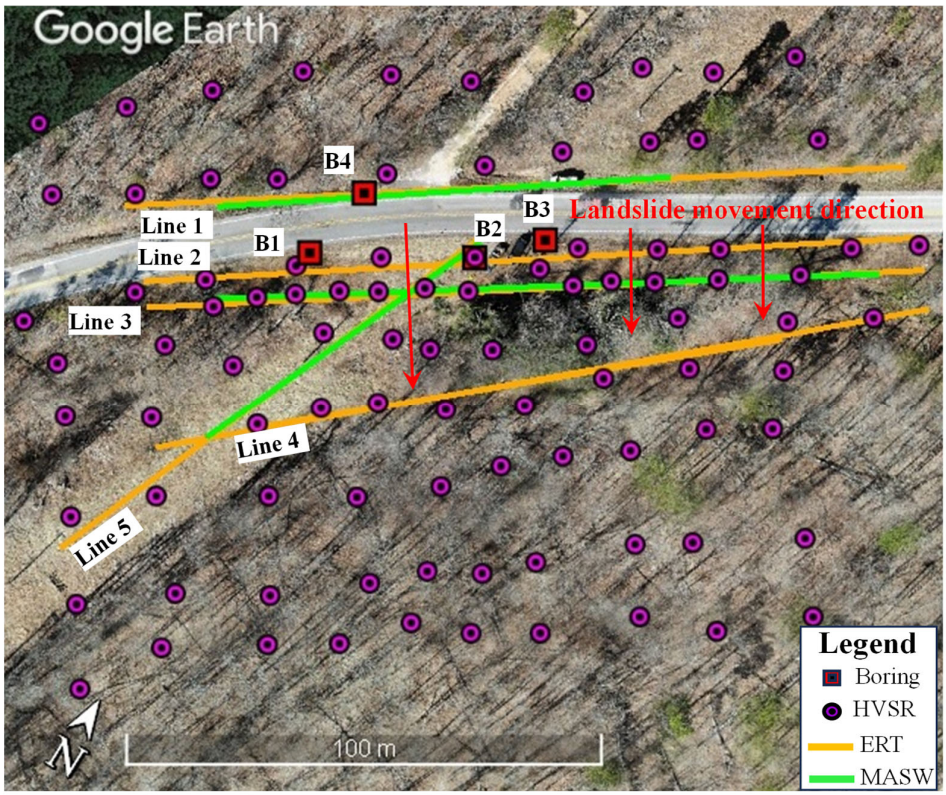


**Figure 1.** Geophysical field measurement layout.


**Figure 2.** A sample longitudinal crack observed on the pavement.

### 3.1. MASW measurements

A linear array of 48, 4.5 Hz vertical geophones with a uniform spacing of 1 m or 2 m between geophones, respectively, for lines parallel and perpendicular to the slope were used for MASW measurements in a rolled along manner. A 5.4 kg sledgehammer was used to generate Rayleigh-type surface waves by striking an aluminum plate overlain by a rubber damping pad. A minimum of three blows were stacked at each source offset to increase the reliability and the signal-to-noise ratio of the experimental data. For each array setup, waves were generated at multiple source offsets to decrease uncertainties regarding selecting the fundamental mode of propagation and also to be able to generate different shear wave velocity profiles for each array setup. Rayleigh waves were generated at 17 source offsets for each array setup, including a source offset 1 m off each end and every 6 m within the array. Several subarrays from the 48-geophone spread were created for processing. Each was composed of 24 geophones and moving along the general array to generate the pseudo-2D Vs cross section.

The experimental MASW raw dispersion data with multiple source offsets were combined and processed in Matlab using the frequency domain beamformer method (Zywicki and Rix 1999). The fundamental mode of propagation for Rayleigh waves was then defined and used as an input for the inversion process. Multiple source offsets aid in identifying potential near-field effects, selecting the fundamental mode of surface wave propagation, and estimating dispersion uncertainty. For each dataset, the maximum spectral peak was automatically picked in the frequency-wavenumber domain to reduce user bias. The extracted dispersion data generally showed the fundamental mode to be dominant across most frequencies of interest. Figure 3a shows a sample experimental dispersion data and Figure 3b presents the final fundamental mode dispersion curve used as input for the inversion process. The Rayleigh dispersion data and frequency associated with the peak HVSR was inverted using the Geospy software package to develop the 1D shear wave velocity (Vs) profile. The boring log information was used as a guide to determine the parameterization for the inversion process. The 1D Vs profiles generated for each subarray survey line were combined to develop a pseudo 2D Vs cross-section for each MASW survey line.

### 3.2. ERT measurements

ERT surveys were performed along five different survey lines, including four survey lines perpendicular to the slide and one survey line parallel to the slide. The SuperSting R8/IP Wifi resistivity meter from Advanced Geoscience Inc. (AGI) was used to collect the ERT data for each survey line. The ground was moist during the tests with good contact resistance. For each survey line, testing was performed using 56 surface electrodes spaced either 2 m (a total array length of 110 m) or 3 m (a total array length of 165 m) apart. Two-dimensional dipole-dipole and strong gradient survey configurations were used to collect data for each survey line. A strong-gradient array is an optimized array, which uses electrode configurations derived from the Wenner and Dipole-Dipole arrays to collect data. This provides a measured dataset with a good vertical and horizontal resolution, allowing for the identification of vertical and horizontal discontinuities. The relative location of each electrode was surveyed using a Nikon Total Station with the true location of the end of each line surveyed using a Trimble Geo7x centimeter GPS unit.

The raw ERT data sets were inverted using AGI's EarthImager2D software. Electrode elevations from the total station were included in the inversions. The misfits between measured and modeled resistivity data for each profile, as measured by the root mean square error (RMSE) were minimized in the inversions keeping under 5% after enough trials. Up to 20% of measured data were removed following this criterion.

### 3.3. HVSR measurements

HVSR measurements were performed using three-component Nanometrics Trillium Compact seismometers with a flat response from 100 Hz to 20 secs. HVSR testing was performed with a minimum recording time of 15 minutes for each individual station. HVSR measurements were acquired along the MASW and ERT lines and in a grid pattern within the entire slide area. The raw HVSR data were processed in general accordance with SESAME (2004). If peak(s) of HVSR measurement meets the requirements of a true and reliable peak (SESAME 2004), then it was used for further processing to estimate depth to the sharp impedance contrast in the Vs profile (i.e., the contact between soft soil material and the stiff bedrock) of the site using the equation below.

$$H = V_{s,avg} / 4f \quad (1)$$

In this equation, $V_{s,avg}$ is the average Vs of the materials above the sharp impedance contrast, $H$ is the thickness of sediments above the sharp impedance contrast, and $f$ is the frequency associated with the HVSR peak. The average Vs of materials above the sharp impedance contrast can be determined either from the

MASW testing or by back calculation from the boring information. Here, the average Vs was determined using the Vs profiles generated from the MASW testing.

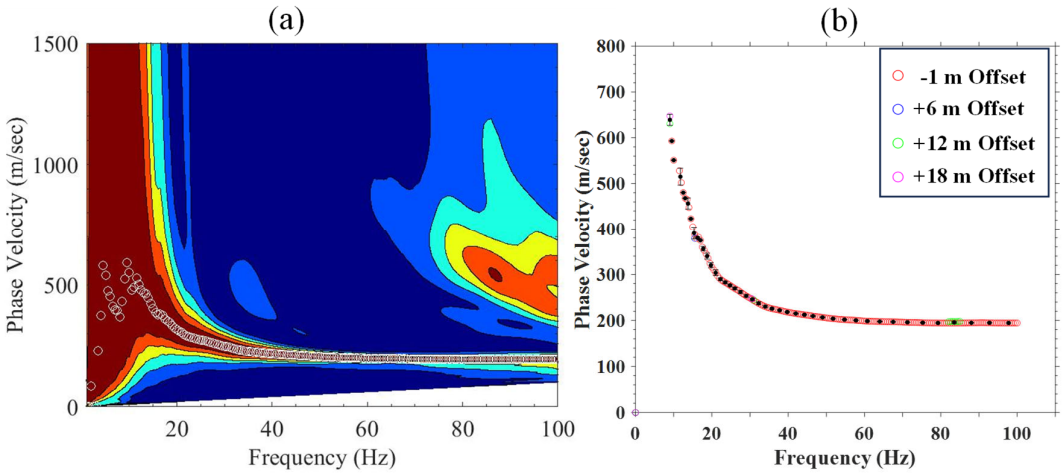


**Figure 3.** Typical experimental dispersion data points (a) raw and (b) refined.

## 4. Results

The results of the MASW and ERT surveys along with the HVSR recordings are presented in this section.

### 4.1. MASW result

Presented in Figure 3 are the pseudo 2D shear wave velocity (Vs) cross-sections for survey lines 1, 3, and 5, along with the soil stratigraphy encountered in the borings B2 and B4. For each line, the pseudo 2D Vs cross-sections were generated by combining the individual 1D Vs profiles.

From the pseudo 2D Vs cross-section for Line 1 in Figure 3, the subsurface layering of this survey line can be divided into two main layers, including medium dense to very dense soils/highly weathered rock followed by a more competent (weathered rock layer in the boring) rock unit with Vs ranging between 650-1100 m/s. The bedrock elevation is shown with a solid black line in Figure 3. From the pseudo 2D Vs cross-section for Line 1, depth to the weathered rock unit is almost consistent (ranging between 10-12 m) from the start of the survey line to an approximate distance of 75 m. For the rest of the survey line, the depth to the weathered rock unit shallows slightly, as shown in Figure 3. Comparing depth to the weathered rock unit from the MASW and borehole B4, depth to this layer is slightly underestimated from the MASW method. This is likely due to the elevation difference between the location where the MASW array was placed (in the ditch on the north side of the highway) and the boring B4 location. Also, a thin layer of clay was observed in borehole B4 at depth which is located between highly weathered and weathered shale; therefore, it wasn't detected in MASW section.

From the pseudo 2D Vs cross-section for Line 3 in Figure 3, the subsurface layering of this survey line can also be divided into two main layers. These two layers are separated by a solid black line, as shown in Figure 3. From the ground surface to a depth ranging between 9-12 m, subsurface layering includes medium dense to very dense soils/highly weathered rock with a shear wave velocity about 350 m/s. This is followed by a more competent rock unit with Vs ranging between 650-1000 m/s, which corresponds well with the weathered rock layer encountered in the boring. Depth to the competent rock unit is approximately 10-12 m below ground surface (bgs) along this survey line but shallows slightly toward the end of the survey line. This is similar to the findings of Line 1, where depth to the weathered rock unit shallows slightly toward the end of the survey line. Depth to the weathered rock layer is very critical for this project because, according to the inclinometer readings, the zone of displacement matches the depth where the weathered rock unit is observed in the MASW results. In this regard, the inclinometer readings at B2 and an example 1D Vs profile from a location close to B2 are shown in Figure 4a and b, respectively. From this figure, it is apparent that the zone of displacement (depth<11 m) from the inclinometer corresponds well with the increase in Vs at that depth in the 1D Vs profile, which is related to the weathered rock unit. Therefore, the location of the weathered rock unit is of primary importance for this project.

Like survey Line 1, the subsurface layering of survey Line 5 up to 15 m depth is comprised of two main layers, including medium dense to very dense soils/highly weathered rock followed by a more competent (weathered rock layer in the boring) rock unit. From the start of the survey line to an approximate distance of 60 m, the depth to the weathered rock unit is approximately 7.5 m bgs. However, depth to the weathered rock unit increases toward the end of the survey line, with depths ranging between 10-13 m. Overall, depth to the weathered rock unit shallows considerably moving down the slope. Survey line 5 provides the most insightful

cross-section since it was conducted along the slope direction and captures more variation in bedrock depth. The increased depth to competent rock toward the end of the line likely indicates weathering and erosion of the bedrock. The transition from shallow bedrock to deeper and more variable bedrock depth appears to correlate with the observed slope instability and movement. Accounting for these bedrock depth changes and incorporating the spatial variability into slope stability models could improve prediction of unstable areas.

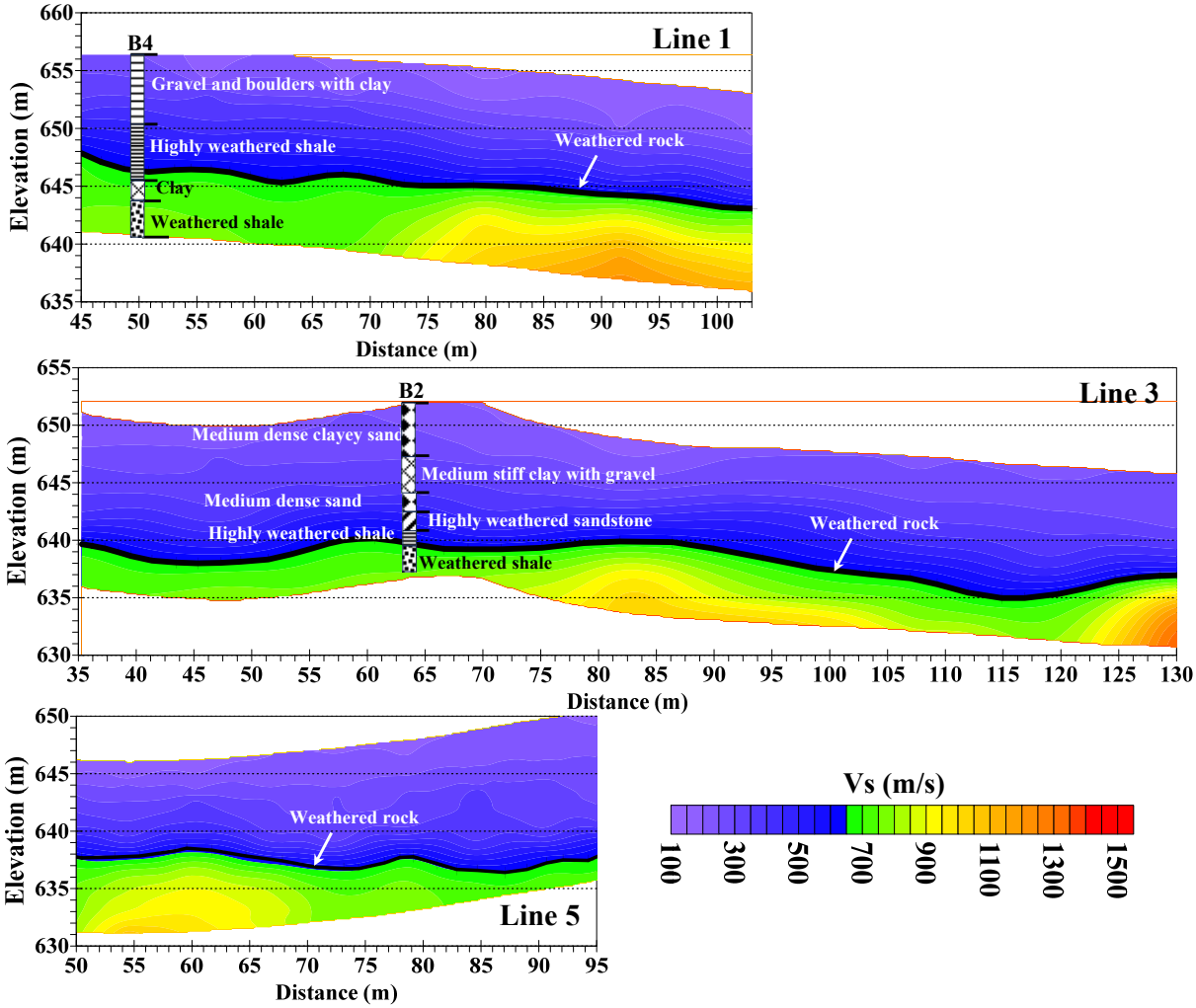


**Figure 4.** Pseudo 2D Vs cross-sections from MASW for survey lines 1, 3, and 5, along with information from the borings B2 and B4.

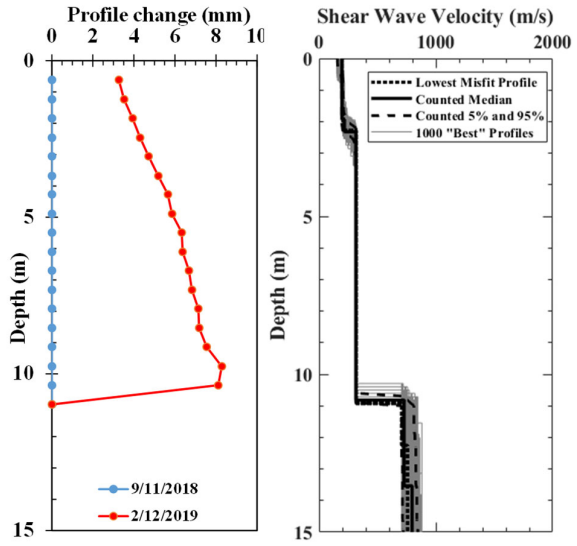


**Figure 5.** Comparison of the inclinometer readings and 1D Vs profile. a) Inclinometer readings at B2, blue readings on September 11, 2018, and red readings on February 12, 2019, b) An example 1D Vs profile from a location close to B2.

## 4.2. ERT result

2D resistivity cross sections for survey lines 1-4 from the ERT testing are presented in Figure 5. Moreover, for Lines 1 and 3 depths to the weathered rock unit identified from the MASW measurements is shown in the 2D resistivity plot. Additionally, to help interpret the ERT results, several vertical guidelines (red dashed lines) that correspond to the wet spots and springs are shown in this figure. These four ERT lines are presented in one figure because they have the same array length (~165 m), and approximately the same starting and ending locations. The result for ERT survey line 5 is shown separately in Figure 6. The main goal of the ERT testing was to determine the location of the water table and/or highly saturated areas within the slide.

From the 2D resistivity profile for Line 1 on the north side of the highway in Figure 5, a very low resistive zone (zone with light and dark purple color) with resistivity lower than 80 Ohm-m is observed from an approximate distance of 30 m to 60 m at a very shallow depth (0-2 m) to a depth of approximately 20 m below ground surface. Very low resistive zones such as this with resistivity values approximately less than 80 Ohm-m are likely related to the water saturated zones of the slide (Mauritsch et al. 2000). From the 2D resistivity profile for Line 1 in Figure 5, it is observed that the very low resistive zone of this survey line starts in the soil layers and extends to the weathered rock unit. This indicates that the fractures in the shale rock unit are likely filled with water and/or the shale rock has a similar resistivity to the overlying soil, leading to a very low resistivity for shale materials. This very low resistive zone in the 2D resistivity plot for Line 1 matches the location of two wet spots/seeps observed on the north side of the highway alignment, as illustrated in the orthomosaic image in Figure 5. Additionally, another very low resistive zone (with a much smaller size) is observed toward the end of this survey line, from an approximate distance of 90 m to 110 m. This very low resistive area from 6-15 m deep is likely related to water sitting on top of or just into the bedrock layer.

From the 2D resistivity profile for Line 2 located next to the south side of the highway in Figure 5, a very low resistive zone is observed from an approximate distance of 85 m to 105 m at depths ranging from 13-23 m. Similarly, from the 2D resistivity plot for Line 3, which is 12 m away on the south side of the highway and is very close to Line 2, a very low resistive zone (zone with light and dark purple color) is observed from an approximate distance of 80 m to 105 m at depths ranging from 10-25 m. These zones correspond quite well with several wet spots and springs observed further down the slide on the south side of the highway, as shown in the orthomosaic image in Figure 5.

From the 2D resistivity profile for Line 4 in Figure 5, a very big low resistive zone is observed from an approximate distance of 45 m to 115 m at depths ranging from 15-35 m. This zone agrees quite well with the two wet spots and springs observed further down the slide, as illustrated in the orthomosaic image in Figure 5. In addition, the elevation of the springs observed at the bottom of the slope are at approximately 630 m, which matches well with the elevation of the top of the low resistive zone. Moreover, several very low resistive zones with much smaller sizes are detected very close to the ground surface from an approximate distance of 70 m to the end of this survey line. Shown in Figure 6 is the 2D resistivity plot for survey line 5. This ERT survey line was conducted approximately South-North along the slide. From this figure, zones with very low resistivity (zones with light and dark purple color) are observed along almost the entire survey line. However, depth to these low resistive zones varies considerably throughout the survey line. From the start of the survey line to an approximate distance of 50 m, the very low resistive zone is related to depths ranging from 5-15 m. But, from distance of 50 m to the end of the survey line, depth to the very low resistive zone increase, ranging from 10- 20 m. In other words, depth to the very low resistive zones shallows drastically as moving down the slope. The depth of the low resistive zone matches well with the depth to bedrock determined from the MASW testing in the area, meaning the low resistive zone is associated with the bedrock.

Overall, using the ERT measurements, the low resistive zones within the slide are detected. For the survey line located on the north side of the highway alignment (Line 1), the primary very low resistive zone is located on the west of the tested survey line. However, for all the survey lines located on the south of the highway alignment (Lines 2, 3, and 4), the highly saturated zones are located on the east side of the tested survey lines and near or below the bedrock elevation. These findings agree well with the wet spots and springs that have been observed during the field measurements. It should also be highlighted that depths to these highly saturated zones determined from the ERT testing are likely associated with some uncertainty, and these depths could alter during different seasons depending on the precipitation rate.

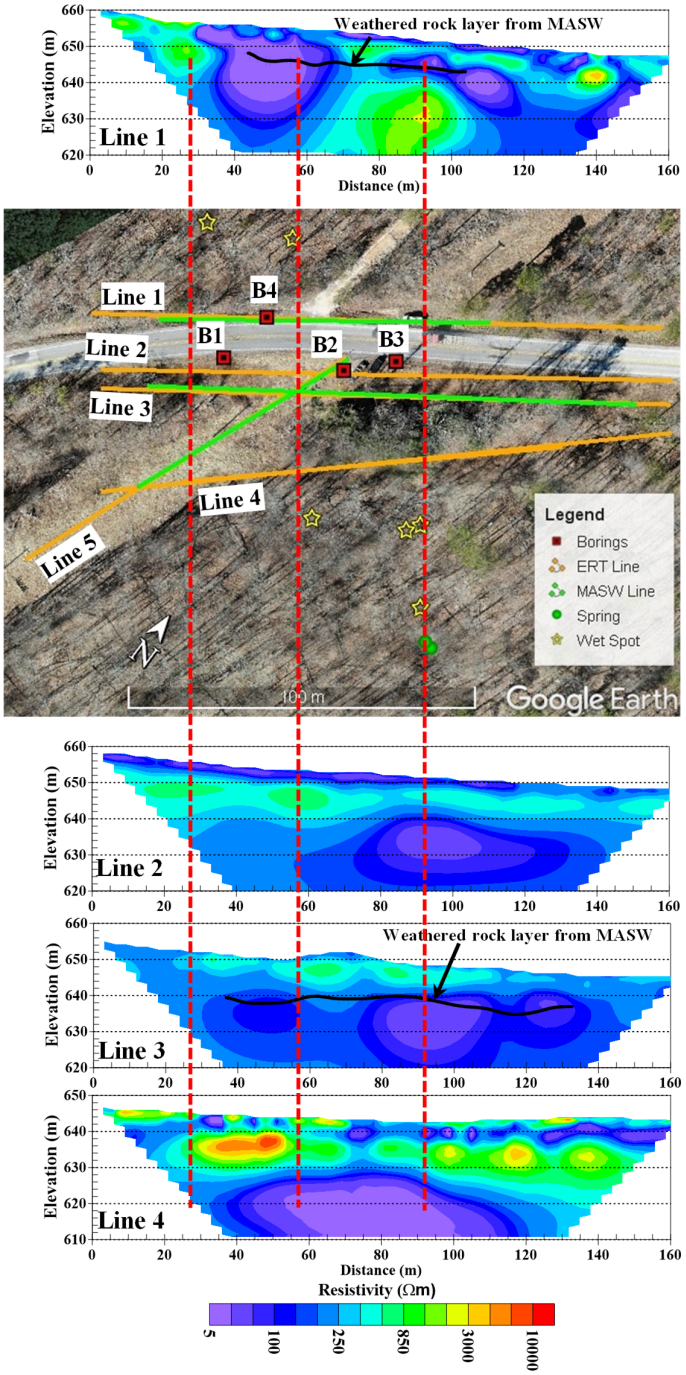


**Figure 6.** 2D resistivity profiles for Lines 1-4.

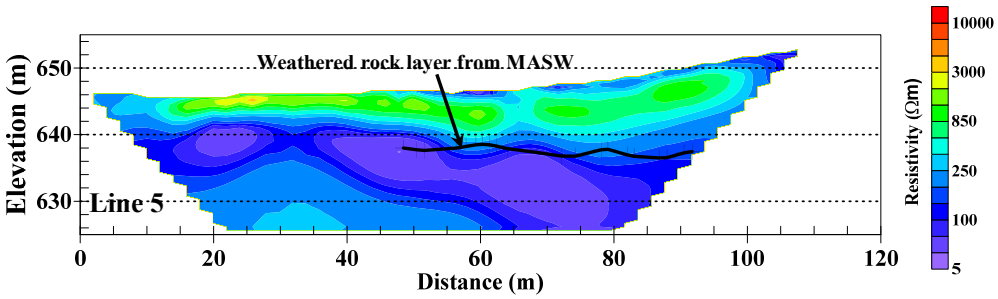


**Figure 7.** 2D resistivity profiles for Lines 5.

### 4.3. HVSR result

Extensive HVSR measurements were collected to determine the variation of depth to the weathered rock unit across the slide area. From these measurements, site HVSR peak frequency (f) was determined at each station ranging between 7.5-70 Hz, and then depth to weathered bedrock was estimated using equation (1). The time-averaged shear wave velocity of the materials above the sharp impedance contrast ($Vs_{,avg}$) was estimated based on the MASW measurements.

Depth to the weathered rock unit determined from the HVSR and MASW methods were then utilized to generate 3D maps of depth to the weathered rock layer and its variation within the slide. These maps include a 3D map of surface elevation, bedrock elevation as shown in Figure 7.

In addition to the information regarding the weathered rock location and its variation across the slope area, the geometry of the slope area (surface elevations) is required for accurate estimates of bedrock elevation. In this respect, the elevation data from GPS and total station readings were combined with the information from the Digital Elevation Model (DEM) derived from the ArcGIS Online maps of the area to create a full 3D surface elevation plot.

Figure 7a shows the 3D map of the elevation of the ground surface while Figure 7b shows the elevation of bedrock. Using these contour maps, depth to bedrock can be derived for any location of interest within the slide area. From the 3D map of the bedrock elevation, it is apparent that the bedrock elevation generally follows the surface elevation for most of the slide area. However, examining the variation of bedrock elevation in the contour map in Figure 7b, depth to bedrock is higher on the north side of the site near to the highway and shallows as moving down the slope. The thicker soil and highly weathered rock stratum underlying the highway alignment likely experiences reduced shear strength when saturated, with its increased weight on the sloped topography contributing to gravitational driving forces triggering mass movement. In addition, the friction force along the critical slide surfaces can decrease when materials get saturated. The variable soil and weathered bedrock thicknesses characterized across the slide area using extensive HVSR measurements enables improved mapping of destabilizing weight distributions across the irregular bedrock morphology.

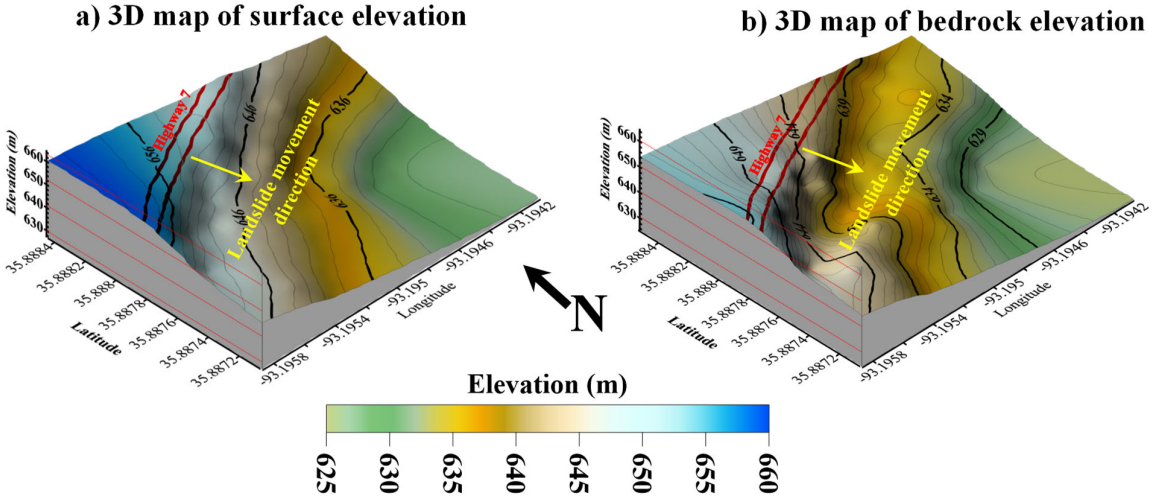


**Figure 8.** 3D maps for the Jasper slide. a) 3D map of surface elevation, b) 3D map of bedrock elevation.

## 5. Discussion

The combined geophysical approach utilizing MASW, ERT, and HVSR provided supplementary information on landslide geology, hydrogeology, and stability. The MASW survey detected a layered subsurface of soil and highly weathered bedrock underlain by more competent rock. Depth to weathered bedrock became slightly shallower moving downslope, likely indicating that the deeper saturated soil on the top of the slope tends to slide along the interface between soil and rock. This aligned with slope inclinometer data showing displacement of soil and weathered rock zone at shallower depths above more competent rock layer.

ERT imaging revealed variable saturation levels across the slide, with very low resistivity anomalies indicating groundwater accumulation zones and water pathways. North of the highway, an extensive water table near the surface feeds visible seeps. To the south, deeper saturation occurred near the soil-bedrock interface, a possible source of springs and wet spots further downslope. Low resistivity anomalies were also detected in saturated fractures within the clay-rich weathered shale bedrock.

Extensive HVSR soundings provided high resolution bedrock depth contours essential for evaluating stability models. Geophysics constrained a highly irregular and sloping bedrock surface to the north likely initiating shear surface development and slope movement. Shallow soil

to the south explains lack of failure in the bottom of the slope.

While some depth and property variations occurred between methods due to measurement specifics and processing assumptions, the complementary geophysical data furnished an excellent 3D framework model to analyze mechanisms and conditions enabling ongoing slope distress. Compared to conventional borehole sampling, integrated geophysics offered more efficient and sustainable landslide evaluation at larger scales relevant for remediation strategies.

## 6. Conclusions

A multi-method geophysical program provided critical details on landslide geometry, hydrogeology, and kinematics necessary for hazard assessment and mitigation along failing slopes. Testing combined MASW, ERT, and HVSR surface-based techniques along a distressed highway segment near Jasper, Arkansas. The key conclusions include:

- MASW detected a variable bedrock depth that became progressively shallower downslope, aligning with inclinometer data to validate failure plane location.
- ERT mapped zones of high moisture content and seepage pathways sourced from springs feeding groundwater flow along the slip surface.
- ERT was not able to accurately resolve the bedrock depth in many areas of the site potentially leading to errors if only ERT was used at the site. This may be due to the highly fractured shale being saturated with water leading to a very low resistivity for this material making it difficult to resolve the bedrock/soil interface.
- HVSR imaging efficiently revealed complex and sloping bedrock morphology useful to detect subsurface problematic zones.
- Comprehensive geophysical model constrains factors contributing to slope movement for designing stabilizing measures.
- Integrated testing provides superior 3D framework compared to sparse borehole sampling for landslide evaluation.

This multi-method geophysical approach offers more efficient, sustainable practice for assessing slope hazard and stability compared to traditional borehole sampling. The comprehensive subsurface model provided by this study better characterizes the factors contributing to slope movement for designing stabilizing measures. Similar methodology could be considered when assessing slope distress or planning infrastructure routes crossing rugged terrain.

## Acknowledgements

The authors are grateful for the financial support provided from ARDOT from the TRC1803 Project.

## References

Adamski, J. C. 1995. “Environmental and hydrologic setting of the Ozark Plateaus study unit, Arkansas, Kansas, Missouri, and Oklahoma”, National Water-Quality Assessment Program, 94(4022).

Alonso-Pandavenes, O., Torrijo, F. J., Garzón-Roca, J., and Gracia, A. 2023. “Early Investigation of a Landslide Sliding Surface by HVSR and VES Geophysical Techniques Combined, a Case Study in Guarumales (Ecuador)”, Appl. Sci., 13(2), 1023. https://doi.org/10.3390/app13021023

Ávila-Barrientos, L., Yegres-Herrera, L. A., and Flores-Estrella, H. 2023. “Characterization of landslides in Federal Highway 1D, Baja California, Mexico, using seismic noise records and the HVSR method”, Nat. Hazards, 1-19. https://doi.org/10.1007/s11069-023-06053-3

Bichler, A., Bobrowsky, P., Best, M., Douma, M., Hunter, J., Calvert, T., Burns, R. 2004. "Three-dimensional mapping of a landslide using a multi-geophysical approach: the Quesnel Forks landslide" Landslides, 1, 29-40. http://doi.org/10.1007/s10346-003-0008-7

Braden, A. K. 2015. “Geologic map of the Mt. Judea quadrangle, Newton County, Arkansas”, Arkansas Geological Commission. Arkansas. gov Geology webpage.

Harba, P., Pilecki, Z., and Krawiec, K. 2019. “Comparison of MASW and seismic interferometry with use of ambient noise for estimation of S-wave velocity field in landslide subsurface”, Acta Geophys., 67(6), 1875-1883. https://doi.org/10.1007/s11600-019-00344-9

Hussain, Y., Hamza, O., Cárdenas-Soto, M., Borges, W. R., Dou, J., Rebolledo, J. F. R., and Prado, R. L. 2020. “Characterization of Sobradinho landslide in fluvial valley using MASW and ERT methods”, REM, Int. Eng. J., 73, 487-497. https://doi.org/10.1590/0370-44672019730109

Imani, P., Tian, G., Hadiloo, S., and Abd El-Raouf, A. 2021. “Application of combined electrical resistivity tomography (ERT) and seismic refraction tomography (SRT) methods to investigate Xiaoshan District landslide site: Hangzhou, China”, J Appl Geophy., 184, 104236. https://doi.org/10.1016/j.jappgeo.2020.104236

Jongmans, D., and Garambois, S. 2007. “Geophysical investigation of landslides: a review”, Bull. Soc. géol. Fr, 178(2), 101-112. https://doi.org/10.2113/gssgfbull.178.2.101

Mauritsch, H.J., Seiberl, W., Arndt, R., Römer, A., Schneiderbauer, K., and Sendlhofer, G.P. 2000. “Geophysical investigations of large landslides in the Carnic Region of southern Austria”, European Journal of Environmental and Engineering Geophysics, 5(3), 143-156. https://doi.org/10.1007/PL00013716

Petley, D. 2012. “Global patterns of loss of life from landslides”, Geology, 40(10), 927-930. https://doi.org/10.1130/G33217.1

Rahimi, S., Wood, C. M., and Bernhardt-Barry, M. 2021. The “MHVSR technique as a rapid, cost-effective, and non-invasive method for landslide investigation: case studies of Sand Gap and Ozark, AR, USA”, Landslides, 18(8), 2705-2720. https://doi.org/10.1007/s10346-021-01677-7

Samodra, G., Ramadhan, M. F., Sartohadi, J., Setiawan, M. A., Christanto, N., and Sukmawijaya, A. 2020. “Characterization of displacement and internal structure of landslides from multitemporal UAV and ERT imaging”, Landslides, 17(10), 2455-2468. https://doi.org/10.1007/s10346-020-01428-0

SESAME European Research Project. 2004. “Guidelines for the implementation of the H/V spectral ratio technique on ambient vibration. Measurements, processing and interpretations”. Project No. EVG1-CT-2000-00026.

Zywicki, D. J., and Rix, G. J. 1999. “Frequency-wavenumber analysis of passive surface waves. In Symposium on the Application of Geophysics to Engineering and Environmental Problems”, Society of Exploration Geophysicists, 75-84. https://doi.org/10.4133/1.2922675